JOURNAL OF SPACECRAFT AND ROCKETS
Vol. 38, No. 4, July–August 2001

Photometry of Global Positioning System Block II and IIA Satellites on Orbit

Henry F. Fliegel* and Lori F. Warner†
The Aerospace Corporation, El Segundo, California 90245
and
Frederick J. Vrba‡
U.S. Naval Observatory, Flagstaff, Arizona 86002

Observations have been taken at the U.S. Naval Observatory of the colors and brightness of two Global Positioning System Block II and two Block IIA satellites against calibrated standard stars. Spacecraft logarithmic brightness falls off with phase angle almost linearly, as with the moon or Mercury, but more steeply: 0.04–0.05 astronomical magnitudes per degree. Knowing this value may permit a significant refinement of the Global Positioning System solar force model. The colors of all of the satellites are much redder than they would be if the optical properties of the surfaces remained as measured in the factory and so show the effects of degradation in space. The hypothesis that most of the degradation is caused by self-contamination by effluent from the spacecraft bodies is examined and rejected, being incompatible with the relative brightnesses in the yellow, red, and near infrared.

Introduction

THE degradation of satellite surfaces in space is a grave concern to all designers and especially to the Global Positioning System (GPS) because such degradation reduces the power delivered by the solar arrays and shortens the useful vehicle lifetime. There is now considerable literature both on the effect of contaminants outgassed by the GPS vehicle bodies and on the measured power loss for each space vehicle (SV) over time (e.g., Refs. 1–4). There are many possible causes for the degradation of spacecraft surfaces besides contaminants, e.g., darkening of the solar array cover glass by charged particles, micrometeoric bombardment, and chemical attack by ionized molecules. No direct measurements of the optical properties of GPS satellites as they change with age have previously been available, and so no comparison of theoretical predictions of degradation with observations has been possible. Therefore the U.S. Naval Observatory, in cooperation with The Aerospace Corporation, has begun a program of astronomical measurements of the color and brightness of GPS satellites as a function of their apparent angle from the sun. Such measurements rely on an all-sky catalog of photometric standard stars, whose brightness as seen on Earth is known in absolute units (watts/square meter) to a few percent and whose relative brightnesses are known to a few tenths of a percent.[5] Both satellite positions and the brightnesses at selected wavelengths (colors) are measured, and those brightnesses are reduced to the astronomical system of apparent magnitudes. In this now classical system, the fainter the star, the larger the number that specifies the apparent magnitude; and the scale of brightness is logarithmic, the chosen logarithmic base being the fifth root of $100 = 2.512$. So a star of magnitude 10.0 is 100 times brighter than a star of magnitude 15.0. In engineering terms one astronomical magnitude equals 4 dB. Because astronomers have carefully removed stars that vary in brightness from catalogs of photometric standard stars, these astronomical measurements provide benchmarks of the brightness and therefore the reflectivity of each satellite at known times, with a stability and a precision that equals or even exceeds that which could be obtained in a laboratory. These measurements also provide a way to refine solar force models, which are essential to precise ephemeris generation and which depend critically on the optical properties of the satellites.[6,7]

Received 20 October 2000; revision received 24 March 2001; accepted for publication 24 March 2001.

*Project Engineer, Global Positioning System Directorate.
†Senior Member of the Technical Staff, Satellite Navigation Department.
‡Staff Astronomer.

The photometric observations can easily be compared to model calculations because of the way in which GPS spacecraft are oriented. The antennas always point toward the Earth and define the body-fixed $+Z$ direction; and each SV is maneuvered so that the sun is in the spacecraft's plane of symmetry, called the XZ plane. The Block II and IIA vehicles, which we observed, are always oriented by means of so-called noon turns so that the angle between sun and antennas in the XZ plane is between 0 and 180 deg. This angle is therefore the SV/Earth/sun phase angle, which we call γ in this paper; when this angle exceeds 166 deg, the spacecraft is in eclipse, because the Earth's radius subtends about 14 deg at GPS altitude. For our purposes another angle is more useful: the SV/observer/sun angle, which we call δ, equal to 180 deg minus the angle of reflection of light to the observer from the solar panels when they are normal to the light from the sun (see Fig. 1). Over the range of our observations, the two angles γ and δ do not differ by more than 10 deg.

Observations

The U.S. Naval Observatory telescope of 1.0-m aperture in Flagstaff, Arizona, was used to perform optical photometry of four GPS satellites—SV 15 and 17 (Block II) and 25 and 38 (Block IIA)—on the nights of 21, 22, and 24 March 1999 universal mean time. These satellites were in eclipse season so that they could be observed through the largest possible range in phase angle. A Tektronix 1024×1024 charge-coupleddevice (CCD) camera with a 0.68-arcsecond pixel scale was used as the detector, giving an 11.5×11.5 arcminute field of view. The filters are standard for astronomical work and are the Johnson B (blue) and V (visual, or yellow) and the Cousins R (red) and I (near infrared).[8] On each night, six or seven standard stars were observed to determine atmospheric extinction (the absorption of light by the Earth's atmosphere) and to put the observations onto the standard photometric system. Photometry of the standard stars was accomplished using synthetic circular apertures appropriate for the atmospheric seeing each night (typically 1.8 arcseconds) in the image processing software package.

The telescope was pointed in advance at a star field that the SV was to cross, and the stars were tracked as the SV trailed across the field of view. The satellites crossed the CCD field of view in 23–32 s of time, depending on the satellite distance and the angle between the line of sight and the SV orbital velocity. The exposure time was 5 s of time for each observation. Each exposure was determined by opening and closing a shutter with timing accuracy of 0.01 s of time or 0.2% of the exposure time. On each night six or seven standard stars were measured at different elevation angles, and the atmospheric extinction coefficient was estimated for that night. Because the observing sessions were fairly short, the error

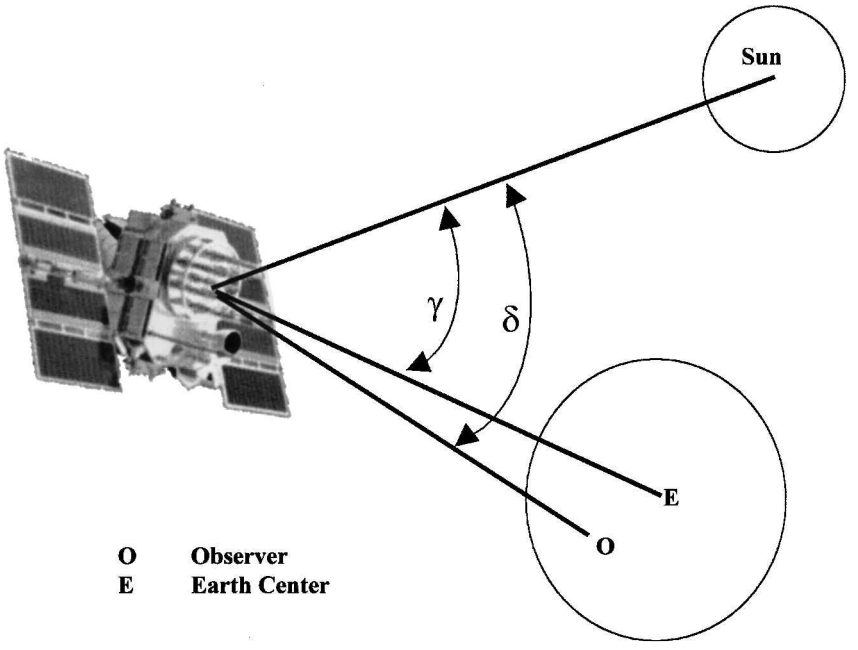

Fig. 1 Angles γ (sun/Earth/center) and δ (sun/Earth/observer).

Table 1 Effective wavelengths: filter plus CCD camera

	Wavelength, nm	
Color	Nominal	Calculated (true)
B	440	429
V	550	565
R	640	640
I	790	804

caused by changing atmospheric extinction was limited to about 0.01 magnitudes per air mass.

The same circular synthetic aperture that was used for the standard stars each night was also used for the satellite tracks. With typical track lengths of 270 pixels and aperture diameters of 12 pixels, approximately 22 independent measures of track brightness would have been obtained for each exposure, but usually this number was reduced to 19 or 20 measurements because field stars lay close to the track and blended with it. Sky values were determined for each measure in an annulus of several pixels around the measurement aperture by using the mode value of these pixels effectively to exclude the parts of the satellite track going through the annulus. Because each satellite track is known both in time (5.00 ± 0.01 s of time) and length ($\pm$one pixel), the effective exposure time for each 12-pixel-diam measurement aperture was determined.

The effective wavelengths (colors) of the observations depend on two factors: the transmission bandpass of the filters that were used and the quantum efficiency of the CCD camera as a function of wavelength. We convolved the filter manufacturer's transmission curves with the CCD manufacturer's quantum efficiency curves to arrive at the effective wavelengths of the filter-camera combination and obtained the results in Table 1.

However, as we shall see, the spacecraft themselves are very red; because the filter bandpasses are about 20 nm wide, the true effective wavelengths for the spacecraft observations are likely to be 2–5 nm higher than the calculated values given in Table 1. The observations themselves are given in Table 2 and shown in Figs. 2–5.

The "magnitudes (observed)" have been corrected for atmospheric extinction and for background sky brightness, and then the "magnitudes (corrected for range)" have been normalized to a standard distance of 20,000 km from the observer, assuming the inverse square law of brightness and using calculated ranges from The Aerospace Corporation's Trajectory Analysis and Orbit Determination Program. To a good first approximation, the range-corrected magnitudes fall off linearly with phase angle. The brightness of the moon in astronomical magnitudes also is a linear function of phase angle, being brightest at the full (phase = 180 deg) and declining by about 0.027 magnitudes per degree, and solid astronomical bodies such as Mercury and the satellites of Jupiter show similar behavior.[9,10] The GPS brightness curves have a steeper slope than the moon, perhaps because of the effect of shadows cast on the SV body by antennas and other large protuberances; the slope is typically about 0.04–0.05 magnitudes per deg over the range 130–166 deg. The range from 166 to 180 deg is unobservable because the spacecraft are in eclipse. The slopes are approximately equal in all colors, although there is a tendency in these observations for the slope in B to be highest.

Comparing Observed with Predicted Brightnesses

As seen from the Earth, there are three major SV surfaces in view: 1) the solar panels, 10.87 m^2 in area; 2) the forward bulkhead, sheathed in orange Kapton, 2.88 m^2; and 3) the solar panel masts, 0.98 m^2 (Ref. 6). The solar panels of the Block II vehicles, like SV 15 and 17, have an active (or fully populated) area of 7.20 m^2 with a net reflectance when new of 0.23 and an unpopulated area of 3.67 m^2 and a reflectance of 0.07, according to Rockwell International; and the Block IIA vehicles, like SV 25 and 38, have fully populated panels. Using Rockwell International's spectral reflectance curves for the active solar panel surfaces and the orange Kapton and assuming the sun to be a black body with effective temperature 5800 K, we computed the predicted astronomical magnitudes of Block II and IIA vehicles at 20,000 km distance, for phase angle 180 deg, at the beginning of life (Table 3).

We see that the color of a newly launched Block II or Block IIA GPS spacecraft should be almost white, corresponding to a star of spectral class A0 or A2. The extremely blue solar panels almost compensate for the extremely red color of the orange Kapton on the SV body. However we see from Table 2 that the presently observed colors are very red, that all brightnesses (even in the I band) are fainter than predicted, except for the anomalously bright SV 38, and that the present brightnesses diminish smoothly from I through R and V to B. Evidently this behavior is caused by the aging of the SV surfaces in space. The V and I measurements especially show the spacecraft to be progressively fainter with age (see Figs. 2–5); and the two measured R magnitudes are consistent with this behavior.

Comparing Observed Colors to Contamination Predictions

In two important papers[3,4] Rockwell International engineers examined the possible causes for the decrease in electrical power from GPS solar panels with age in space. After briefly discussing charged

Table 2 Observations and linear fit results

γ Angle, deg	Magnitude observed	Observed magnitude error, 1σ	Magnitude corrected for range	Magnitude straight line computed	Residual (observed minus computed)	Linear fit slope	Intercept at 180 deg
			SV 15—22 March 1999—B band				
124.729	15.17	0.10	15.047	14.947	0.100	0.0625	11.493
133.975	14.29	0.07	14.176	14.369	−0.193	±0.0036	±0.129
143.256	13.88	0.06	13.770	13.789	−0.019	——	——
152.506	13.47	0.05	13.359	13.211	0.147	——	——
161.660	12.81	0.04	12.680	12.639	0.040	——	——
170.643	12.16	0.04	12.003	12.078	−0.075	——	——
			SV 15—22 March 1999—V band				
121.664	13.30	0.05	13.169	13.272	−0.103	0.0388	11.006
130.886	13.03	0.05	12.915	12.913	0.002	±0.00498	±0.209
140.163	12.87	0.05	12.761	12.553	0.208	——	——
149.430	12.30	0.05	12.185	12.193	−0.009	——	——
158.624	11.86	0.05	11.738	11.836	−0.098	——	——
			SV 15—22 March 1999—I band				
118.653	11.83	0.04	11.689	11.707	−0.018	0.0431	9.063
127.804	11.34	0.04	11.224	11.313	−0.088	±0.00274	±0.113
137.068	11.08	0.04	10.968	10.913	0.054	——	——
146.377	10.72	0.04	10.613	10.512	0.101	——	——
155.572	10.32	0.04	10.197	10.116	0.081	——	——
164.678	9.73	0.04	9.594	9.724	−0.130	——	——
			SV 17—21 March 1999—B band				
97.111	16.33	0.18	16.259	16.216	0.043	0.0542	11.724
105.704	15.52	0.11	15.466	15.750	−0.285	±0.00204	±0.104
114.345	15.56	0.10	15.502	15.282	0.220	——	——
122.968	14.84	0.07	14.791	14.815	−0.024	——	——
131.557	14.45	0.06	14.392	14.349	0.043	——	——
140.017	13.94	0.06	13.877	13.891	−0.014	——	——
148.239	13.69	0.05	13.607	13.445	0.162	——	——
155.897	13.14	0.04	13.040	13.030	0.010	——	——
162.318	12.76	0.04	12.627	12.682	−0.055	——	——
165.775	12.56	0.03	12.395	12.495	−0.100	——	——
			SV 17—21 March 1999—V band				
94.272	14.53	0.05	14.454	14.520	−0.067	0.0445	10.703
102.823	14.41	0.04	14.347	14.139	0.207	±0.00171	±0.0914
111.456	13.79	0.03	13.737	13.755	−0.018	——	——
120.092	13.25	0.03	13.196	13.370	−0.174	——	——
128.702	12.99	0.03	12.937	12.987	−0.050	——	——
137.223	12.66	0.02	12.599	12.608	−0.008	——	——
145.543	12.34	0.02	12.272	12.237	0.035	——	——
153.448	12.12	0.02	12.026	11.885	0.141	——	——
160.397	11.77	0.03	11.649	11.576	0.074	——	——
165.112	11.38	0.02	11.226	11.366	−0.140	——	——
			SV 17—21 March 1999—I band				
91.439	13.06	0.03	12.981	12.893	0.088	0.0408	9.278
99.955	12.52	0.04	12.455	12.545	−0.090	±0.00139	±0.0777
108.579	12.21	0.03	12.149	12.193	−0.044	——	——
117.224	11.86	0.03	11.804	11.840	−0.037	——	——
125.838	11.50	0.03	11.445	11.489	−0.044	——	——
134.398	11.26	0.02	11.200	11.139	0.060	——	——
142.793	10.94	0.03	10.868	10.797	0.072	——	——
150.868	10.67	0.02	10.584	10.467	0.117	——	——
158.239	10.35	0.02	10.239	10.166	0.073	——	——
163.922	9.88	0.02	9.740	9.934	−0.194	——	——
			SV 17—22 March 1999—B band				
107.283	15.14	0.11	15.09	15.58	−0.488	0.0476	12.117
115.945	15.50	0.17	15.45	15.16	0.283	±0.00504	±0.238
124.606	15.00	0.10	14.95	14.75	0.199	——	——
133.227	14.61	0.09	14.55	14.34	0.212	——	——
141.712	14.02	0.08	13.96	13.94	0.019	——	——
149.920	13.64	0.07	13.55	13.55	0.006	——	——
157.525	13.18	0.07	13.07	13.19	−0.118	——	——
163.727	12.92	0.07	12.78	12.89	−0.114	——	——
			SV 17—22 March 1999—V band				
95.779	14.71	0.08	14.642	4.436	0.206	0.0442	10.718
104.400	13.98	0.07	13.922	14.055	−0.133	±0.00224	±0.123
113.066	13.82	0.07	13.764	13.673	0.091	——	——
121.721	13.11	0.06	13.058	13.291	−0.232	——	——
130.356	12.86	0.06	12.801	12.909	−0.108	——	——
138.905	12.62	0.06	12.560	12.532	0.027	——	——

(Continued)

Table 2 Observations and linear fit results (continued)

γ Angle, deg	Magnitude observed	Observed magnitude error, 1σ	Magnitude corrected for range	Magnitude straight line computed	Residual (observed minus computed)	Linear fit slope	Intercept at 180 deg
147.220	12.32	0.06	12.241	12.165	0.076	——	——
155.087	12.00	0.06	11.903	11.818	0.085	——	——
161.912	11.63	0.06	11.504	11.516	−0.012	——	——
			SV 17—22 March 1999—I band				
92.944	13.00	0.05	12.925	12.801	0.124	0.0383	9.469
101.522	12.51	0.04	12.444	12.472	−0.028	±0.00113	±0.0648
110.168	12.13	0.03	12.072	12.142	−0.069	——	——
118.834	11.80	0.04	11.742	11.810	−0.068	——	——
127.485	11.47	0.03	11.421	11.479	−0.058	——	——
136.075	11.21	0.03	11.151	11.150	0.001	——	——
144.480	10.96	0.03	10.888	10.828	0.060	——	——
152.540	10.68	0.03	10.590	10.520	0.070	——	——
159.815	10.33	0.03	10.210	10.242	−0.031	——	——
			SV 17—24 March 1999—V band				
101.812	14.22	0.08	14.164	14.048	0.116	0.0416	10.799
110.510	13.66	0.05	13.612	13.687	−0.075	±0.00204	±0.100
119.240	13.26	0.05	13.206	13.324	−0.118	——	——
127.944	12.93	0.04	12.878	12.962	−0.084	——	——
136.599	12.66	0.04	12.601	12.603	−0.001	——	——-
145.107	12.48	0.04	12.406	12.249	0.157	——	——
153.309	12.18	0.04	12.083	11.908	0.175	——	——
160.772	11.71	0.04	11.583	11.598	−0.015	——	——
166.373	11.37	0.04	11.211	11.365	−0.155	——	——
			SV 17—24 March 1999—R band				
98.922	13.55	0.04	13.482	13.422	0.059	0.0414	10.063
107.607	13.08	0.04	13.030	13.063	−0.033	±0.00152	±0.0787
116.323	12.71	0.03	12.656	12.701	−0.045	——	——
125.043	12.26	0.03	12.212	12.340	−0.127	——	——
133.725	12.07	0.03	12.013	11.980	0.033	——	——
142.295	11.81	0.03	11.741	11.625	0.116	——	——
150.621	11.46	0.03	11.371	11.280	0.091	——	——
158.407	11.12	0.03	11.006	10.957	0.048	——	——
164.848	10.69	0.03	10.548	10.690	−0.142	——	——
			SV 17—24 March 1999—I band				
96.037	12.94	0.04	12.876	12.834	0.042	0.0436	9.177
104.707	12.40	0.03	12.343	12.456	−0.113	±0.00204	±0.105
113.415	12.12	0.03	12.064	12.077	−0.013	——	——
122.138	11.70	0.03	11.645	11.697	−0.052	——	——
130.839	11.38	0.02	11.323	11.318	0.005	——	——
139.457	11.07	0.02	11.009	10.943	0.066	——	——-
147.877	10.80	0.02	10.717	10.576	0.141	——	——
155.904	10.52	0.02	10.412	10.226	0.186	——	——
162.946	10.11	0.02	9.981	9.920	0.061	——	——
167.388	9.57	0.02	9.404	9.726	−0.322	——	——
			SV 25—21 March 1999—B band				
163.125	12.48	0.03	12.369	12.480	−0.111	0.0497	11.739
155.499	13.41	0.04	13.322	12.897	0.425	±0.00481	±0.243
147.106	13.40	0.04	13.337	13.357	−0.020	——	——
138.368	14.00	0.05	13.943	13.835	0.108	——	——
129.500	14.22	0.06	14.161	14.321	−0.160	——	——
120.596	14.36	0.06	14.288	14.808	−0.520	——	——
111.727	15.20	0.11	15.108	15.294	−0.186	——	——
102.943	15.95	0.19	15.834	15.775	0.059	——	——
			SV 25—21 March 1999—V band				
165.320	10.56	0.02	10.438	11.084	−0.646	0.0377	10.530
158.175	11.70	0.02	11.609	11.353	0.256	±0.00475	±0.251
149.957	11.87	0.02	11.796	11.663	0.134	——	——
141.310	12.28	0.02	12.217	11.989	0.229	——	——
132.464	12.60	0.02	12.542	12.322	0.220	——	——
123.563	12.85	0.03	12.785	12.658	0.127	——	——
114.676	13.13	0.02	13.046	12.993	0.053	——	——
105.859	13.34	0.03	13.232	13.326	−0.093	——	——
97.151	13.51	0.03	13.375	13.654	−0.279	——	——
			SV 25—21 March 1999—I band				
160.717	9.64	0.03	9.533	9.678	−0.145	0.0333	9.036
152.762	9.94	0.02	9.859	9.943	−0.084	±0.00230	±0.122
144.221	10.39	0.02	10.326	10.228	0.098	——	——
135.432	10.72	0.03	10.666	10.521	0.145	——	——
126.542	10.98	0.02	10.923	10.817	0.106	——	——
117.643	11.25	0.02	11.178	11.114	0.065	——	——-
108.788	11.48	0.03	11.389	11.409	−0.020	——	——
100.011	11.66	0.03	11.536	11.701	−0.165	——	——

(Continued)

Table 2 Observations and linear fit results (continued)

γ Angle, deg	Magnitude observed	Observed magnitude error, 1σ	Magnitude corrected for range	Magnitude straight line computed	Residual (observed minus computed)	Linear fit slope	Intercept at 180 deg
			SV 38—22 March 1999—B band				
154.540	12.92	0.07	12.639	12.628	0.010	0.0879	10.391
148.236	13.42	0.06	13.161	13.182	−0.021	±0.00116	±0.0425
140.862	14.08	0.08	13.842	13.830	0.012	——	——
132.858	14.75	0.10	14.532	14.533	−0.002	——	——
			SV 38—22 March 1999—V band				
156.309	10.74	0.06	10.444	10.551	−0.107	0.0633	9.053
150.491	11.32	0.06	11.055	10.919	0.136	±0.00831	±0.286
143.400	11.63	0.06	11.392	11.368	0.024	——	——
135.577	12.03	0.06	11.809	11.862	−0.053	——	——
			SV 38—22 March 1999—I band				
152.594	9.32	0.03	9.049	9.058	−0.009	0.0793	6.885
145.874	9.86	0.04	9.607	9.591	0.017	±0.00199	±0.0697
138.222	10.42	0.03	10.190	10.198	−0.008	——	——
			SV 38—24 March 1999—V band				
148.189	11.58	0.04	11.326	11.282	0.045	0.0510	9.660
140.447	11.82	0.04	1.590	11.677	−0.087	±0.00939	±0.378
132.194	12.36	0.04	12.139	12.097	0.042	——	——
			SV 38—24 March 1999—R band				
150.599	10.02	0.03	9.760	9.802	−0.042	0.069	7.772
143.098	10.64	0.03	10.400	10.319	0.081	±0.00894	±0.337
134.986	11.06	0.03	10.841	10.879	−0.039	——	——
			SV 38—24 March 1999—I band				
152.892	9.67	0.02	9.405	9.393	0.012	0.0349	8.446
145.683	9.86	0.02	9.622	9.645	−0.023	±0.00263	±0.0925
137.712	10.16	0.02	9.935	9.924	0.011	——	——

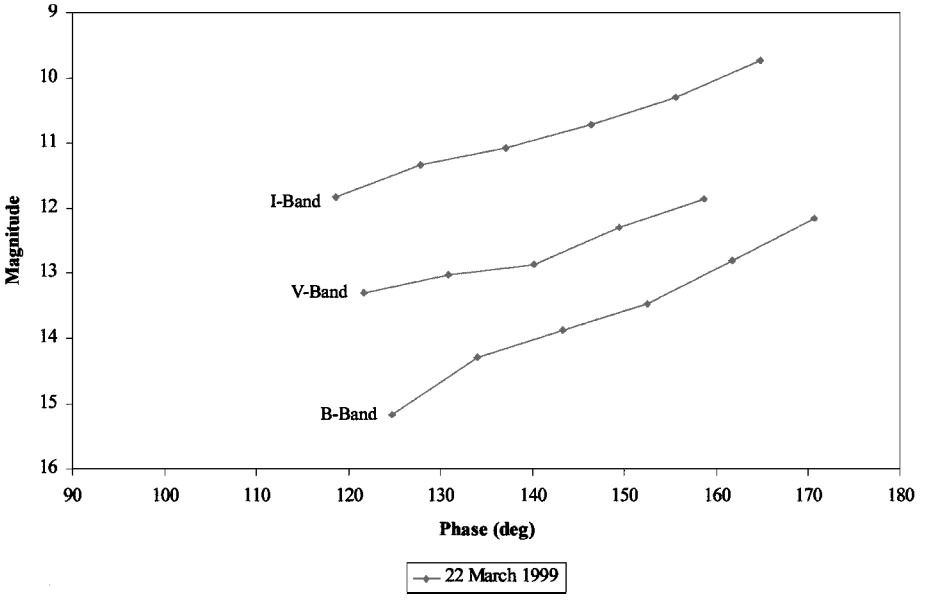

Fig. 2 SV 15.

particle bombardment from the Van Allen belts as a possible factor,[3] these studies focused on contaminants emitted from inside the spacecraft hull as the most likely cause of this decrease. We therefore have explored the possibility that the progressive dimming and reddening of the spacecraft which our observations indicate might be caused primarily by such contaminants.

In Table 4 we give our calculation of absorption in astronomical magnitudes, in the B, V, R, and I filters, to be expected for a given path length through a layer of contaminant of uniform thickness over the SV body, based on Fig. 8 of Ref. 3: "Contamination film effect on transmitted sunlight." To be sure, it is highly unlikely that actual contaminants would be in a uniform layer, but such a simple model provides a good starting point. In Table 4 path length is not the same as contaminant thickness. The authors of Ref. 3 were concerned to calculate solar panel loss of power, and sunlight travels once through the contaminant to reach the panels. But a terrestrial observer sees sunlight that has traversed the film twice, once entering and once exiting after reflection from the panels; although the ray enters normal to the plane of the film, it exits obliquely; its path length increased by the secant of 180 deg minus the phase angle δ (SV/observer/sun). So the path lengths used to calculate Table 4 are the actual contaminant thicknesses multiplied by the factor (1-sec δ): typically, for our observations, by 2.30.

In the I band absorption is small for any reasonable contaminant thickness. Therefore, the color indices B-I, V-I, and R-I are the best criteria of the contaminant hypothesis. From Table 2 the average

value of presently observed B-I is 3.0 magnitudes for Block II and 3.6 magnitudes for Block IIA and are calculated to be about −0.1 at the beginning of life (Table 3). This is consistent with a contaminant thickness of about 1.8–2.0 μ (Table 4). By itself, such a thickness might be plausible. According to Fig. 7 of Ref. 3, it would correspond to a power loss of about 25%, which is reasonable. But then the corresponding color indices V-I and R-I would be only 1.0 and 0.1 magnitudes, respectively, whereas the observed values are V-I = 1.6 and R-I = 0.8 magnitudes for Block II and V-I = 1.7 and R-I = 0.3 magnitudes for Block IIA. The discrepancy is far too large to be explained as observational error. Because the contaminants absorb very strongly in the blue and very little in the yellow and red, according to Ref. 3, they cannot produce the gradual descent from I through R and V to B that we see in the observations.

If we now pass from the simplified model of a uniform thickness of contaminants to a more realistic scenario, the discrepancy between the observed brightnesses and reported SV power loss, on the one hand, and the contaminant hypothesis, on the other, becomes more acute. As Ref. 3 explains, "the performance of a string of solar cells is governed by the performance of the worst cell in the string." Patches of contaminants over the solar cells would have a far larger effect on power than on observed brightness or color. The rather modest power losses reported for GPS spacecraft, on the average, 3.1% per year, are not consistent with the faint B magnitudes we observed if the contaminant is patchy.

Our conclusion is that contaminants are not the primary cause of GPS SV surface degradation, at least so far as optical properties are concerned. The question whether contaminants are responsible for most of the power loss needs to be reexamined.

Table 3 Expected GPS astronomical magnitudes at 180-deg phase angle (from manufacturer-supplied materials properties)

Wavelength	Block II (e.g., SV-15, 17)	Block IIA (e.g., SV-25, 38)
B (blue)	8.90	8.69
V (visible)	8.84	8.71
R (red)	8.70	8.54
I (infrared)	9.00	8.84
B-V	0.06	−0.02
V-I	−0.16	−0.13
B-I	−0.10	−0.14

Table 4 Calculated loss in astronomical magnitudes caused by contaminant (based on Fig. 8, Ref. 3)

	Contaminant thickness, μ				
Wavelength	1.6	1.8	2.0	2.2	2.4
B	3.0	3.4	3.9	4.3	4.8
V	1.0	1.2	1.4	1.6	1.8
R	0.3	0.4	0.5	0.6	0.7
I	0.3	0.3	0.4	0.4	0.5
B-V	2.0	2.3	2.5	2.8	3.0
V-I	0.7	0.9	1.0	1.1	1.3
B-I	2.7	3.1	3.5	3.9	4.3

Specularity and the Solar Force Model

In calculating the force of solar radiation on GPS spacecraft, the angular distribution of sunlight reflected from each surface has previously been approximated as the sum of two beams, one perfectly diffuse (Lambert scattering) and the other purely specular.[6] With a Lambert surface, the intensity of the reflected light is equal for all angles of reflection, but the total amount of light reflected at an angle α to the normal to the surface diminishes with cosine α because the total apparent area of the surface is foreshortened. Sunlight normal to a surface when specularly reflected imparts a force equal to $2\,AE/c$, where A is the true area of the surface in square meters, E the solar power constant (about 1365 W/m^2), and c the speed of light. The factor of 2 appears because (so to speak) the momentum imparted by each photon to the surface is the momentum of the incoming photon plus (or minus, observing the sign convention) the momentum of the reflected photon. For Lambert scattering the factor 2 is reduced to 1 plus $\frac{2}{3}$. The convention that divides the reflected light into a Lambert plus a specular component is quantified by two optical parameters: the reflectivity ν, ranging from 0 (black) to 1 (white); and the specularity μ, where μ ranges from 0 (purely diffuse reflection) to 1 (a mirror surface). The value of μ for most SV surfaces is poorly known even at the beginning of life, let alone after years of aging in space. Moreover, the observations here reported show that real spacecraft reflect light very differently than the convention would imply.

Sunlight strikes the solar panels normal to the surface, and the angle of reflection is the supplement of the δ angle (SV/observer/sun) listed in Table 2. For the forward bulkhead, because the GPS spacecraft are always maneuvered to face the Earth, the angle of incidence is the supplement of the γ angle (sun/SV/Earth), and the angle of reflection is close to zero because the observer is at most 10 deg or so from the Earth's center as seen from the SV. By the principle of optical reversibility, the situation is equivalent to that in which the angle of incidence is nearly zero, and the angle of reflection is the γ angle. We here approximate by treating the γ and δ angles as equal; by doing this, we can equate the slope of the phase/magnitude plots

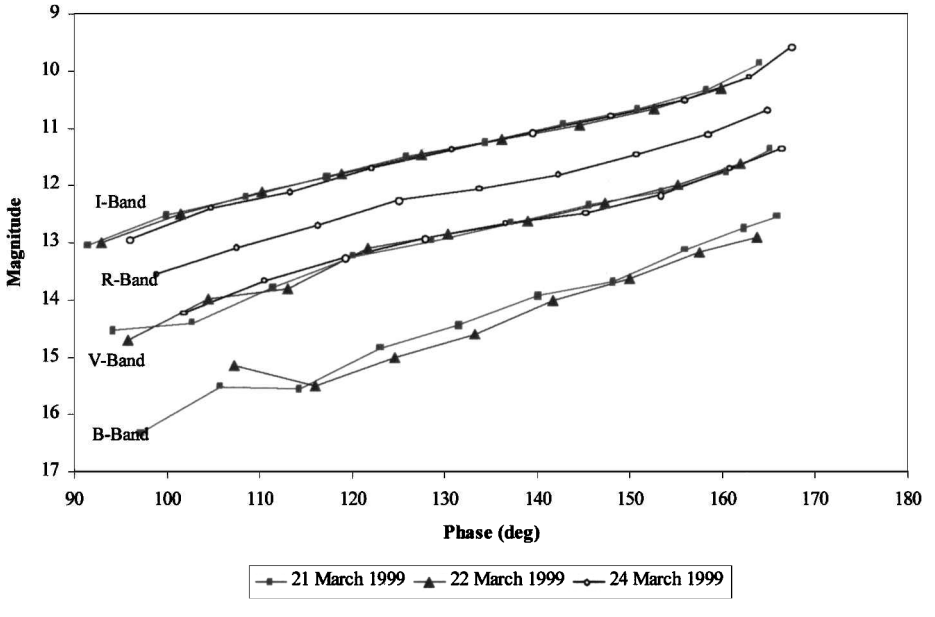

Fig. 3 SV 17.

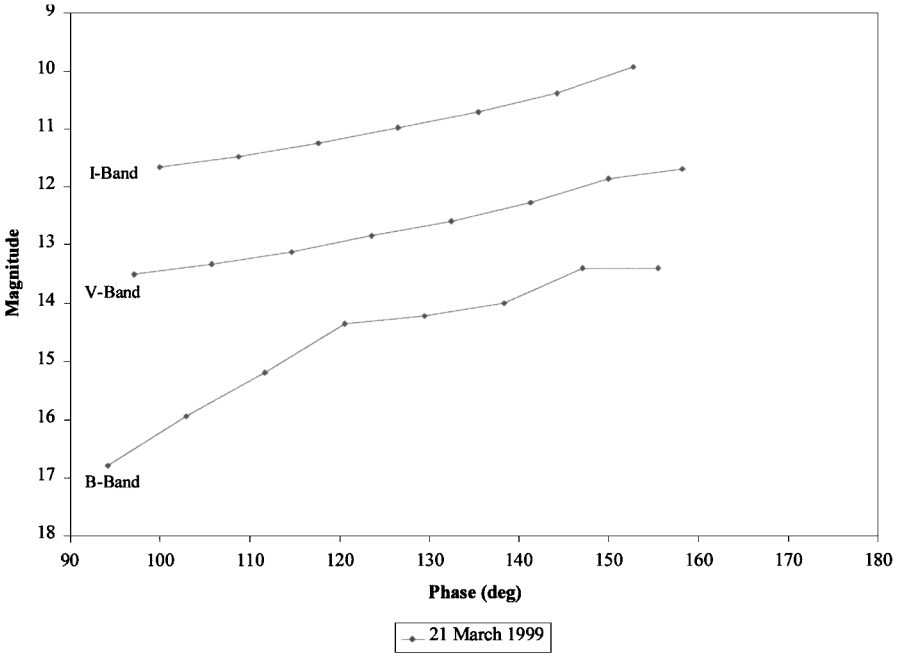

Fig. 4 SV 25.

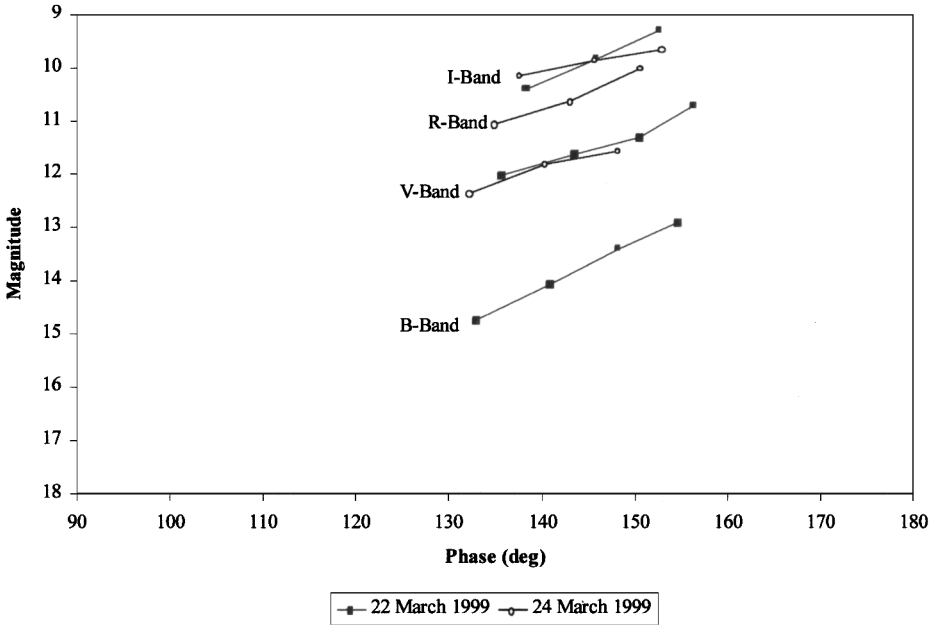

Fig. 5 SV 38.

of Figs. 2–5 to the distribution of reflected energy as a function of the angle of reflection and merge the solar panels and forward bulkhead (and the smaller surfaces also) as though they were one surface. The +X side is nearly invisible from Earth and −Z aft bulkhead quite so, but because these surfaces are covered with orange Kapton they presumably have the same optical properties as the forward bulkhead.

By our method we are including the effect of shadowing of antennas, etc., on the forward bulkhead in the quantity μ. In the oldest GPS solar force models, called ROCK4 and ROCK42, the effect of shadowing was calculated separately by subtracting the area of each shadow from that of the surface on which it falls. However, this is a very questionable procedure.[6] The light so subtracted does not just disappear, but at most angles of illumination it is scattered to some other SV surface and reflected. Given the uncertainties of our problem, we believe that the procedure presented next for calculating an effective value of μ is at least as accurate as any other available.

If the intensity of reflected light is a function F of the angle of reflection A, then the vertical component of the force caused by reflected sunlight is proportional to the quotient Q of two integrals; we have

$$Q = \frac{2\pi \int_0^{\pi/2} F(A) \cos^2 A \sin A \, dA}{2\pi \int_0^{\pi/2} F(A) \cos A \sin A \, dA} \tag{1}$$

where the denominator is the total radiation over a hemisphere of reflected light obeying the $F(A)$ law, the $\cos(A)$ is the foreshortening factor, and the numerator is the vertical component thereof, diminished by another factor of $\cos(A)$. This quotient Q would have a value of $\frac{2}{3}$ for a hypothetical case of zero slope and a value of one for purely specular reflection. From Table 2 the logarithm of the

function F is about 0.04 or 0.05 astronomical magnitudes per deg, and F itself is e^{-fA}, where f is therefore about 2.1–2.6. For this exponential law of brightness, both integrals can be evaluated analytically; we have

$$Q = \frac{3 + f^2 - 2fe^{-\pi f/2}}{f^4 + 10f^2 + 9} \Big/ \frac{1 + e^{-\pi f/2}}{f^2 + 4} \tag{2}$$

For f between 2.11 and 2.64, Q ranges between 0.81 and 0.84. Now we calculate forces by the following modification of the procedure given in Ref. 6. There is no specular component. The diffuse component for flat surfaces, given as F in Ref. 6, is replaced by the equation

$$F_{1,D} = -0.84(AE/c)\nu \cos\theta \tag{3}$$

where ν is the net reflectivity of the surfaces facing the sun. Because the reflectivities ν of the various surfaces are not nearly so well known, the specularity has gone from being the most doubtful of optical parameters of GPS spacecraft to the best determined.

Estimating the reflectivity of the solar panels is complicated by their color; they reflect only 3% of incident light in the visual part of the spectrum, but the net reflectivity is given by the manufacturer as 0.23, because of the high contributions in the blue (less than 400 nm) and infrared (greater than 1 μ).[11] We currently have no observations in those parts of the spectrum. Not knowing the true value of ν for the solar panels, it is useless to refine those for the other surfaces. We refrain from issuing a T21 model to replace the T20 of Ref. 6 until we have further observations.

Conclusions

GPS Block II and IIA satellites are bright enough to be easily observed with modern astronomical equipment, and the brightnesses can be measured with a precision of a few percent for a range of phase angles from 130 deg or so to the eclipse limit at 166 deg. Like the moon, the GPS satellite brightnesses fall off exponentially with the angle from the antisolar point, but even more steeply than the moon, possibly because of shadowing from antennas, etc. Brightness diminishes by 0.04–0.05 magnitudes per deg of phase angle. The satellites show strong effects of surface degradation and not primarily from contaminants outgassed from the spacecraft body. Measurements in at least four colors, such as the astronomical B, V, R, and I bands, are very valuable to discriminate between contaminant effects and other causes of degradation. The U.S. Naval Observatory is continuing these observations and planning to add measurements into the infrared, to extend the time history of the changes of GPS optical properties.

References

[1]Champetier, R., "Effects of Contaminants on Optical Characteristics of Surfaces," Spacecraft Contamination from Propulsion Systems Workshop, The Aerospace Corp., El Segundo, CA, Sept. 1981.

[2]Stewart, T. B., Arnold, G. S., Hall, D. F., Marvin, D. C., Hwang, W. C., Chandler, R. D., and Martin, H. D., "Photochemical Spacecraft Self-Contamination—Laboratory Results and Systems Impacts," *Journal of Spacecraft and Rockets*, Vol. 26, No. 5, 1989, pp. 358–367.

[3]Tribble, A. C., and Haffner, J. W., "Estimates of Photochemically Deposited Contamination on the GPS Satellites," *Journal of Spacecraft and Rockets*, Vol. 28, No. 2, 1991, pp. 222–228.

[4]Tribble, A. C., "Revised Estimates of Photochemically Deposited Contamination on the Global Positioning System Satellites," *Journal of Spacecraft and Rockets*, Vol. 35, No. 1, 1997, pp. 114–116.

[5]Seidelmann, P. K. (ed.), *Explanatory Supplement to the Astronomical Almanac*, Univ. Science Books, Mill Valley, CA, 1992, pp. 505–539.

[6]Fliegel, H. F., Gallini, T. E., and Swift, E. R., "Global Positioning System Radiation Force Model for Geodetic Applications," *Journal of Geophysical Research*, Vol. 97, No. B1, 1992, pp. 559–568.

[7]Fliegel, H. F., and Gallini, T. E., "Solar Force Modeling of Block IIR Global Positioning System Satellites," *Journal of Spacecraft and Rockets*, Vol. 33, No. 6, 1996, pp. 863–866.

[8]Bessell, M. S., "UBVRI Photometry II: The Cousins VRI System, Its Temperature and Absolute Flux Calibration, and Relevance for Two-Dimensional Photometry," *Publications of the Astronomical Society of the Pacific*, Vol. 91, No. 543, 1979, pp. 589–607.

[9]Fessenkov, V. G., "Photometry of the Moon," *Physics and Astronomy of the Moon*, edited by Z. Kopal, Academic Press, New York, 1962, pp. 99–115.

[10]Allen, C. W., *Astrophysical Quantities*, 2nd ed., Athlone Press, Univ. of London, London, 1963, p. 145.

[11]Porter, W. W., "Solar Force and Thermal Radiation Force Model, Special Task #ST003," Rockwell International, Final Rept. CDRL 001A22, Contract FO4701-83-0031, Seal Beach, CA, April 1994, p. 21.

A. C. Tribble
Associate Editor